Talanta 100 (2012) 377–383

Contents lists available at SciVerse ScienceDirect

Talanta

journal homepage: www.elsevier.com/locate/talanta

Highly sensitive hydrazine chemical sensor fabricated by modified electrode of vertically aligned zinc oxide nanorods

Sadia Ameen [a,1], M. Shaheer Akhtar [b,1], Hyung Shik Shin [a,*]

[a] Energy Materials & Surface Science Laboratory, Solar Energy Research Center, School of Chemical Engineering, Chonbuk National University, Jeonju 561-756, Republic of Korea
[b] New & Renewable Energy Material Development Center (NewREC), Chonbuk National University, Jeonbuk, Republic of Korea

ARTICLE INFO

Article history:
Received 26 June 2012
Received in revised form
31 July 2012
Accepted 2 August 2012
Available online 20 August 2012

Keywords:
ZnO nanorods
Aligned nanostructures
Hydrazine
Chemical sensor
Sensitivity

ABSTRACT

A highly sensitive, reliable and reproducible hydrazine chemical sensor was fabricated using vertically aligned ZnO nanorods (NRs) electrode. The low temperature hydrothermal process was adopted to synthesize the vertically aligned ZnO NRs on fluorine doped tin oxide (FTO) glass. The morphological characterizations revealed the vertical arrangement of highly dense ZnO NRs on FTO substrates. The ultraviolet diffused reflectance spectroscopy (UV-DRS) of aligned ZnO NRs electrode obtained the band gap of ~3.29 eV which was close to that of bulk ZnO nanomaterials. The synthesized aligned ZnO NRs electrode was directly used to elucidate the chemical sensing performance towards the detection of hydrazine by simple current–voltage (*I–V*) characteristics. The aligned ZnO NRs electrode based hydrazine chemical sensor presented a significantly high sensitivity of $\sim 4.42446 \times 10^{-5}$ A mM^{-1} cm^{-2} and the detection limit of ~515.7 μM with a correlation coefficient (*R*) of ~0.73297 and a short response time (10 s). The electrochemical analysis of vertically aligned ZnO NRs electrode in the presence of hydrazine showed the increased current with high height of anodic peak which confirmed the involvement of high electron transfer process via high electrocatalytic activity of the electrode.

1. Introduction

Hydrazine and its derivatives are largely used in various chemical/pharmaceutical industries, agriculture applications, insecticides, herbicides, fuel cells, rocket propellants and explosives [1–2]. However, high doses of hydrazine could cause a serious damage to the central nervous system, kidneys, and liver [3] thus, the chemical and pharmaceutical industries require a reliable and sensitive analytical tool for the detection of hydrazine to cure the ecosystem, environment and human health. So far, the chromatographic, electrochemical, chemiluminesence and spectroscopic methods have been used for the detection of hydrazine and its derivatives [4–5]. Among numerous methods, the electrochemical method provides the advantages of high sensitivity, wide linear range, economical, rapid response, portability and ease of operating procedure [6–7]. The electrochemical method is still a challenge to enhance the electron transfer rate over the surface of working electrode for sensors. Therefore, the modifications of the electrodes with different inorganic and organic nanomaterials could be promising for the reliable and effective detection of harmful chemicals by electrochemical and current–voltage (*I–V*) characteristics.

Zinc oxide (ZnO) nanomaterials have been extensively explored as the most encouraging materials for many optical–electrical and the photovoltaic devices [8–10]. The nanocrystalline ZnO [11] with a wide band gap of ~3.37 eV exhibits high exciton, binding energy, low-cost synthesis, biocompatibility, better electrochemical activities, non-toxicity, chemical and photochemical stability and high-electron communication features [12–14]. Moreover, ZnO nanomaterials based electrodes have shown good electrochemical activities towards chemicals, biomolecules and gases owing to their high-electron transfer characteristics with high electrochemical and photochemical stability [15–16]. Recently, one-dimensional (1D) ZnO nanostructures such as nanorods (NRs), nanobelts (NBs), nanowires (NWs) and nanotubes (NTs) have been studied for fabricating various electrochemical and photoelectrochemical devices due to their sufficiently high surface-to-volume ratio and good electrical characteristics [17–18]. In particular, vertically aligned or arrays of ZnO NRs are the promising materials for optoelectronic, electrochemical, photoelectrochemical and solar devices due to its unique electronic and high surface-to-volume ratio [19]. Thus, 1D ZnO aligned nanostructures could be promising and effective electrodes for sensing applications towards the detection of various chemicals and biomaterials. So far, few literatures have reported on the electrochemical detection of hydrazine and its

* Corresponding author. Fax: +82 63 270 2306.
E-mail address: hsshin@jbnu.ac.kr (H.S. Shin).
[1] Authors contributed equally to this work.

0039-9140/$ - see front matter © 2012 Elsevier B.V. All rights reserved.
http://dx.doi.org/10.1016/j.talanta.2012.08.001

derivatives using ZnO nanostructures based modified electrodes [20–22]. Ni et al. fabricated hierarchical micro/nanoarchitecture ZnO based electrodes for hydrazine sensing with the sensitivity of $\sim$0.51 μA μM^{-1} cm^{-2} [23]. Fang et al. demonstrated the utilization of ZnO nanoflowers modified electrode for the fabrication of hydrazine chemical sensor with a sensitivity of $\sim$3.49 μA μM^{-1} cm^{-2} [24]. Umar et al. reported the electrochemical sensor for the detection of hydrazine over the surface of gold electrode modified with ZnO nanorods [25]. Generally, the formation of ZnO nanostructures often involves complex procedures, sophisticated equipments and a rigid experimental condition which inhibits the sensing properties. In this work, a simple and less expensive low temperature hydrothermal method is used for the synthesis of highly uniform and vertically aligned ZnO NRs on FTO glass substrates. To the best of our knowledge, for the first time the vertically aligned ZnO NRs electrodes have been directly applied for the effective detection of hydrazine through simple current (I)–voltage (V) characteristics. The fabricated vertically aligned ZnO NRs thin film modified electrode is effective for the rapid detection of hydrazine and shows a high sensitivity of $\sim 4.42446 \times 10^{-5}$ A mM^{-1} cm^{-2} and a detection limit of $\sim$515.7 μM with a correlation coefficient (R) of $\sim$0.73297 and a short response time (10 s).

2. Experimental

2.1. Synthesis of vertically aligned ZnO NRs thin film on FTO substrates

Prior to the synthesis of vertically aligned ZnO NRs thin film on FTO substrates, ZnO seeding was performed by spin coating the 0.3 M ethanolic solution of zinc acetate dihydrate (Zn $(CH_3COOH)_2 \cdot 2H_2O$, Aldrich-sigma, 98% assay) at 4500 rpm for 60 s. The ZnO seeded FTO substrates were annealed at 100 °C for 10 min. The vertically aligned ZnO NRs thin film on the seeded FTO substrates was achieved by the hydrothermal method. The equimolar aqueous solution of zinc nitrate hexahydrate (Zn $(NO_3)_2 \cdot 6H_2O$, Aldrich-sigma, 98% assay, 0.08 M) and hexamethylenetetramine ($(CH_2)6\ N_4$, Aldrich-sigma, 98% assay, 0.08 M) was prepared. Polyethylene imine (PEI, Aldrich-sigma, 98% assay, 0.96 g) was added into the reaction mixture with vigorous shaking and the solution was kept on stirring for 1 h at room temperature. Thereafter, the prepared reaction mixture was transferred into a Teflon beaker and ZnO seeded FTO substrates were placed vertically with the non-conducting side of the substrates against the beaker. The Teflon beaker was sealed into a stainless steel autoclave and maintained at 95 °C for 5 h. After completion of the reaction, the autoclave was cooled under flowing water.

2.2. Characterization of vertically aligned ZnO NRs thin film

The morphological observations were studied by using field emission scanning electron microscopy (FESEM, Hitachi S-4700, Japan) and transmission electron microscopy (TEM, JEM-2010-JEOL, Japan). Crystalline structures of the ZnO NRs thin film were studied by X-ray powder diffraction (XRD, Rigaku, Cu-Kα, $\lambda = 1.54178$ Å) in the Bragg angle ranging within 20° and the optical properties were measured by UV-DRS spectrophotometer (2550 Shimadzu, Japan). The structural modifications of vertically aligned ZnO NRs were studied by the Fourier transform infrared (FTIR, Nicolet, IR300) and Raman spectra (Raman microscope, Renishaw). X-ray Photoelectron Spectroscopy (XPS) was performed by using AXIS-NOVA CJ109, Kratos Inc., at a range of 0–800 eV.

2.3. Fabrication and characterization of hydrazine chemical sensor based on vertically aligned ZnO NRs electrode

For hydrazine sensing, the vertically aligned ZnO NRs electrode was used as working and Pt wire as a counter electrode in 0.1 M phosphate buffer solution (PBS, 10.0 ml) for the wide concentrations range of hydrazine from $\sim$0.3 μM to 0.03 M. The hydrazine sensing performance was evaluated by measuring the I–V characteristics using Electrometer (Keithley, 6517 A, USA). The sensitivity of the fabricated hydrazine chemical sensor was estimated from the slope of the current versus concentration from the calibration plot divided by the value of the active area of sensor/electrode. All the sensing experiments were performed at room-temperature. The current response was measured from applied voltage of 1–3 V with the response time of 10 s. The electrocatalytic behavior of the vertically aligned ZnO NRs electrode was studied by the cyclic voltammetry (CV) by using the WPG100 electrochemical measurement system. CV was performed in a three-electrode one compartment cell using vertically aligned ZnO NRs electrodes as working electrode, Pt wire as counter electrode, and an Ag/AgCl reference electrode in 0.1 M PBS (10.0 ml) without and with hydrazine (0.3 μM).

3. Results and discussion

3.1. Morphological characterizations of vertically aligned ZnO NRs

The surface and cross-sectional view of FESEM images are studied to analyze the morphology of ZnO NRs on the seeded FTO substrates, as shown in Fig. 1. The highly dense ZnO NRs could be seen in the surface view image at low magnification (Fig. 1(a)). The high magnification image, as shown in Fig. 1(b), displays the typical hexagonal structure of ZnO NRs with the average diameter of $\sim$200–300 nm. The cross-sectional view (Fig. 1(c, d)) reveals the densely vertically aligned ZnO NRs on FTO substrates. The ZnO NRs possess the average diameter of $\sim$200–300 nm and length of $\sim$3–5 μm. It clearly suggests that the thin layer of ZnO seed significantly results in the uniform vertically aligned ZnO NRs on the FTO substrate with the average thickness of $\sim$5 μm. In support, the vertically aligned ZnO NRs are further characterized by the TEM analysis, as shown in the inset of Fig. 1(b). The typical ZnO hexagonal structure with the average diameter of $\sim$200–300 nm is seen, which is much consistent with the FESEM results. The element mapping images of vertically aligned ZnO NRs are shown in Fig. 2 for Zn and O elements. The homogeneous distribution of the Zn and O elements in vertically aligned ZnO NRs are seen, which confirms the composition of the vertically aligned ZnO NRs.

3.2. Crystalline and structural characterizations of vertically aligned ZnO NRs

Fig. 3(a) shows the XRD patterns of vertically aligned ZnO NRs deposited on the FTO substrate. The grown ZnO NRs exhibit the crystalline peaks of ZnO at 32.2°, 34.8°, 36.6°, 48.1°, 57.3°, 63.4° and 68.6° which match well with JCPDS no. 36-1451 [26]. These patterns are attributed to the typical wurtzite structure of ZnO crystals. However, the diffraction peaks at 26.8°, 34.2°, 51.9°, 55°, 62° and 66.2° are associated with of the FTO substrate [27]. Noticeably, the diffraction peak (101) indicates the preferential orientation due to the vertical growth of NRs on the FTO substrate [28]. Fig. 3(b) shows the UV-DRS spectra and derived band energy plot of vertically aligned ZnO NRs is shown as inset of Fig. 3(b). The ZnO NR obtains the broad intense absorption edge from $\sim$400 nm to lower wavelengths region, originating from a charge-transfer

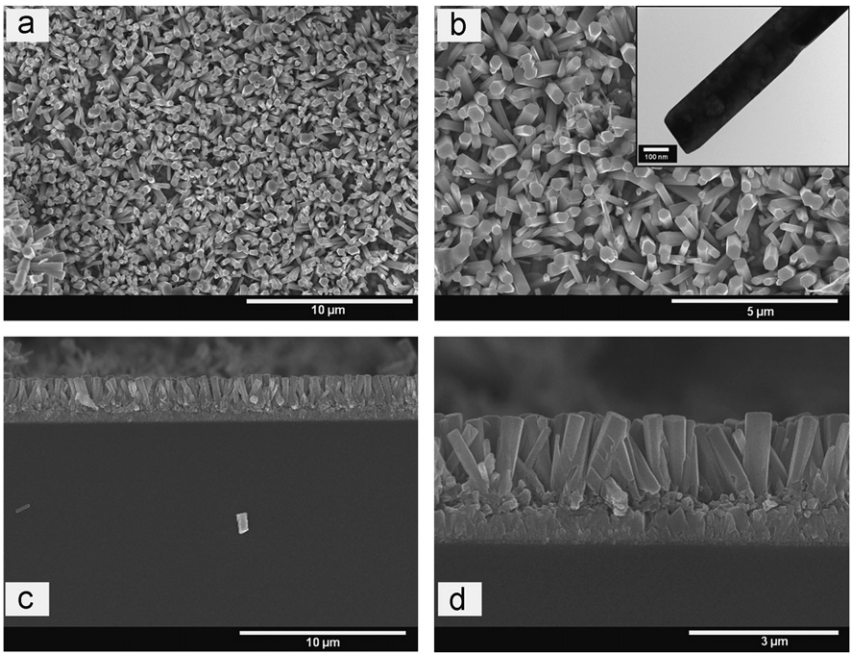

Fig. 1. Surface view (a, b) and cross sectional (c, d) FESEM images of vertically aligned ZnO NRs at low and high magnifications. Inset shows the TEM image of ZnO NRs.

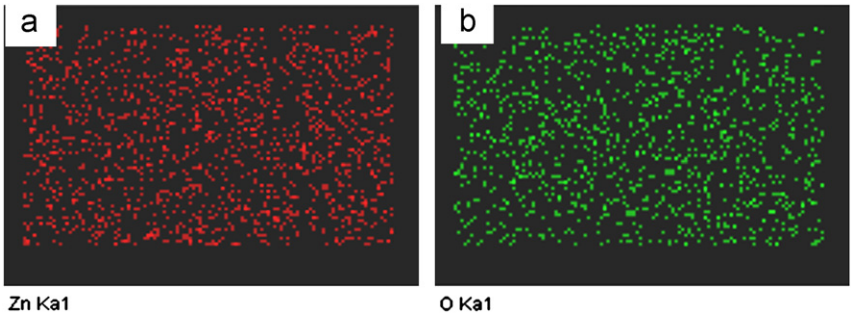

Fig. 2. Elemental mapping of Zn (a) and O (b) for the surface of vertically aligned ZnO NRs.

process from the valence band to the conduction band of ZnO [29]. The band gap of vertically aligned ZnO NRs is calculated as ~3.29 eV which is very close to the band gap of bulk ZnO nanomaterials [30].

The structural properties of vertically aligned ZnO NRs are studied by analyzing the FTIR spectrum, as shown in Fig. 4(a). A very intense IR band at ~554 cm^{-1} is ascribed to the typical Zn–O group of bulk ZnO [31], suggesting that the synthesized ZnO NRs possess pure Zn–O groups. There is appearance of IR peaks at ~3404 and ~1560 cm^{-1} which originated from OH stretching mode and water scissoring vibration or the carboxylate anion asymmetrical stretching respectively [32]. Moreover, the IR band at ~1087 and ~878 cm^{-1} are assigned to υ1 stretching frequency and the bending vibration of nitrate respectively. The investigation of the structural disorder and the defects of the vertically aligned ZnO NRs are elucidated by the Raman scattering spectroscopy, as shown in Fig. 4(b). The presence of strong peak at ~437 cm^{-1} is ascribed to E_2 mode of ZnO crystal which matches with the Raman peak of bulk ZnO crystals [33]. The other two weak peaks at ~331.2 and ~382.1 cm^{-1} are due to the second order Raman spectrum arising from zone-boundary phonons $3E_{2H}$–E_{2L} for wurtzite hexagonal ZnO single crystals and A_{1T} modes respectively. However, the broader peak at ~586 cm^{-1} corresponds to E_1 (LO) mode of ZnO associated with oxygen deficiency in ZnO nanomaterials. It is known that the intense E_2 mode represents the better optical and crystalline properties of ZnO nanomaterials [34]. In our case, the synthesized vertically aligned ZnO NRs possess the high crystallinity with less oxygen vacancies.

Vertically aligned ZnO NRs are further analyzed by the XPS spectroscopy to investigate the chemical structure by taking the Zn 2p and O 1s XPS, as shown in Fig. 5. The doublet peaks with the binding energies at ~1022.2 eV and ~1045.1 eV are recorded in the Zn 2p spectrum (Fig. 5(a)), corresponding to Zn $2p_{3/2}$ and Zn $2p_{1/2}$, respectively. The difference between the two binding energies is estimated as ~23 eV, which is in excellent agreement with the standard reference value of bulk ZnO [35]. Particularly, the appearance of peak at ~1022.2 eV is associated with the Zn^{2+} in ZnO wurzite structure [36]. Noteworthy, the values of Zn 2p binding energy and the difference in binding energies deduce the existence of Zn^{+2} or +2 oxidation state of Zn in ZnO. Fig. 5(b) presents the deconvolution of O 1s XPS spectrum which exhibits the center peak at ~530.4 eV along with three resolved peaks at ~528.4 eV, ~531.5 eV and ~533.7 eV. The binding energies at ~530.4 eV and ~528.4 eV are ascribed to the presence of O_2^- ions on the hexagonal Zn^{2+} ions in wurtzite ZnO structure [37].The higher binding energies at ~531.5 eV and ~533.7 eV are originated due to the oxygen deficiency or oxygen vacancies over the surface of the ZnO materials. Therefore, the

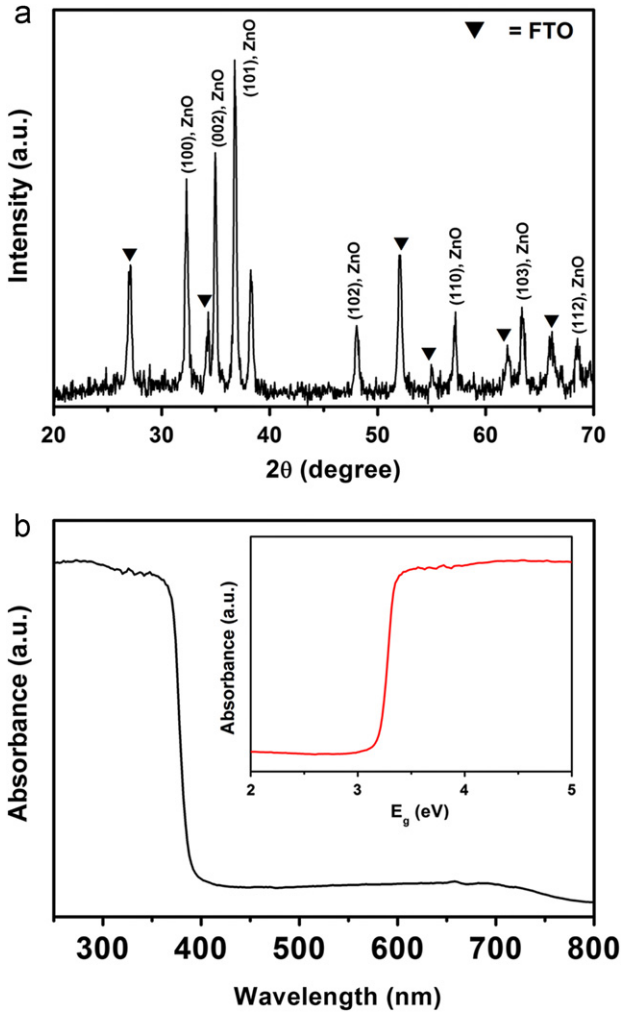

Fig. 3. XRD patterns (a) and UV-DRS spectrum (b) of vertically aligned ZnO NRs.

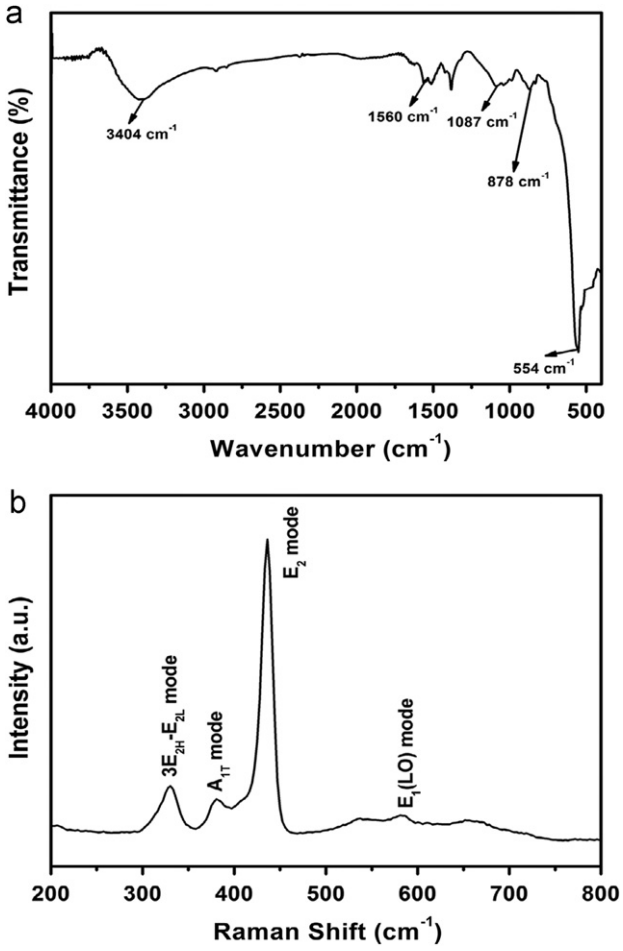

Fig. 4. FTIR (a) and Raman scattering (b) spectrum of vertically aligned ZnO NRs.

XPS of Zn 2p and O 1s spectra has significantly elucidated the Zn–O bonds in ZnO crystals which are associated with Zn^{2+} and O_2^- ions.

3.3. *Hydrazine chemical sensor of vertically aligned ZnO NRs modified electrode*

The electrochemical response of the vertically aligned ZnO NRs electrode is studied to investigate the electrocatalytic activity of vertically aligned ZnO NRs towards hydrazine. Fig. 7(a) shows the typical cyclic voltammogram (CV) of vertically aligned ZnO NRs electrode without and with hydrazine in 0.1 M phosphate buffer (pH=7.0) at a scan rate of 100 mV/s. The sensing response is generally detected by oxidation process of hydrazine. The CV with vertically aligned ZnO NRs electrode displays that the oxidation process begins from ~ -0.38 V and achieves the maximum anodic current of ~ 0.124 mA at -0.109 V. Only the anodic current occurs due to the irreversible electrochemical response towards hydrazine. By looking at the previous literatures, similar electrochemical behavior is found in the present work, and the following proposed reaction is achieved for hydrazine:

$$N_2H_4 + 5/2OH^- \rightarrow 1/2N_3^- + 1/2NH_3 + 5/2H_2O + 2\bar{e}$$

It is noticed that the anodic current of electrochemical system is significantly increased with the addition of hydrazine concentrations in PBS, while a negligible or very low current is observed without hydrazine. The high height and current of anodic peak are usually attributed to a faster electron-transfer reaction in the electrochemical system via high electrocatalytic behavior of electrode [38]. In our work, the vertically aligned ZnO NRs electrode exhibits the increased current with high height of anodic peak in presence of hydrazine, confirming the involvement of high electron transfer process via high electrocatalytic activity of electrode. Thus, the effective oxidative detection of hydrazine is achieved by the vertically aligned ZnO NRs electrode in the electrochemical system.

The current (I)–voltage (V) characteristics have been measured for the fabricated hydrazine sensor with vertically aligned ZnO NRs thin film as the working electrode to evaluate the sensing properties. The fabricated hydrazine chemical sensor based on vertically aligned ZnO NRs thin film as working electrode is illustrated in Fig. 6. A series of I–V characteristics has been tested with various concentrations of hydrazine ranging from 0.3 μM to 0.03 M in 0.1 M PBS for detecting the sensitivity of the fabricated chemical sensor. From Fig. 6, the presence of hydrazine in the fabricated chemical sensor shows an immediate increase in the current ($\sim 4.6 \times 10^{-6}$ A) as compared to without hydrazine based chemical sensor ($\sim 9.3 \times 10^{-7}$ A). The substantial increment in current clearly reveals that a good sensing response towards the detection of hydrazine is associated with the vertically aligned ZnO electrode which might result from its better electrocatalytic activity and fast electron exchange. Moreover, a series of the I–V characteristics is shown in Fig. 7(b) which elucidates the sensing properties of the fabricated hydrazine chemical sensor. With the increase of hydrazine concentrations (0.3 μM–0.03 M), the current has continuously increased, which might originate by the generation of large number of ions and the increase of ionic

strength of the solution with the addition of different concentration of hydrazine. The calibration curve of current versus concentration is plotted to analyze the sensitivity of the fabricated hydrazine sensor, as shown in Fig. 7(c). The current increases with the increase of the hydrazine concentrations up to ~3 mM and then reaches a saturation level as visible in the calibrated plot. This phenomenon occurs due to the unavailability of free active sites over vertically aligned ZnO NRs electrode for hydrazine adsorption at the higher concentration of hydrazine (>0.03 M). The calibration curve is plotted to estimate the sensitivity of hydrazine by taking the slope and dividing by an active area of the electrode (0.5 cm^2). The vertically aligned ZnO NRs electrode based hydrazine chemical sensor shows high and reproducible sensitivity of $\sim 4.42446 \times 10^{-5}$ A mM^{-1} cm^{-2} with a correlation coefficient (R) of ~0.73297, a detection limit of ~515.7 μM and a short response time (10 s). The fabricated hydrazine sensor shows a good linearity in the range of 0.3 μM to 0.3 mM. The stability of hydrazine chemical sensor was determined by measuring the *I–V* characteristics for three consecutive weeks. The fabricated hydrazine sensor did not show any significant decrease in the sensing parameters or properties, confirming the long term stability of the fabricated hydrazine sensor based on vertically aligned ZnO NRs electrode. The obtained sensing parameters such as sensitivity, detection limit and the correlation coefficient have higher values than those obtained in other reported literatures on hydrazine chemical sensor [23,24,39–41]. Enhancement of the sensing properties might be due to the unique vertically aligned morphology of ZnO NRs containing subtle optical, electronic behaviors and strong electrocatalytic activity. Therefore, the vertically aligned ZnO NRs electrode is a promising working electrode for the effective detection of hydrazine.

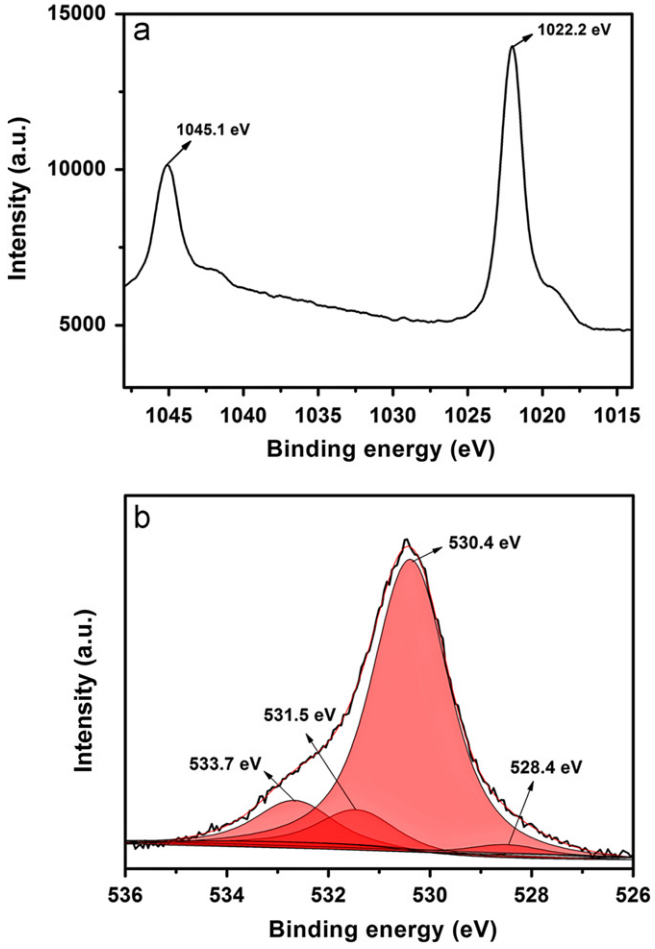

Fig. 5. Zn 2p (a) and deconvoluted O 1s (b) XPS spectra of vertically aligned ZnO NRs.

4. Conclusions

The low temperature hydrothermal process is adopted to synthesize the vertically aligned ZnO NRs on the fluorine doped tin oxide (FTO) glass and applied as working electrode for fabricating a highly sensitive, reliable and reproducible hydrazine chemical sensor. The highly dense ZnO NRs are vertically aligned on the FTO substrates. The UV-DRS of the vertically aligned ZnO NRs electrode exhibits a band gap of ~3.29 eV which is closed to that of bulk ZnO nanomaterials. The synthesized vertically aligned ZnO NRs are directly applied for the chemical sensing performance towards the detection of hydrazine by simple current–voltage (*I–V*) characteristics. The aligned ZnO NRs electrode based hydrazine chemical sensor shows

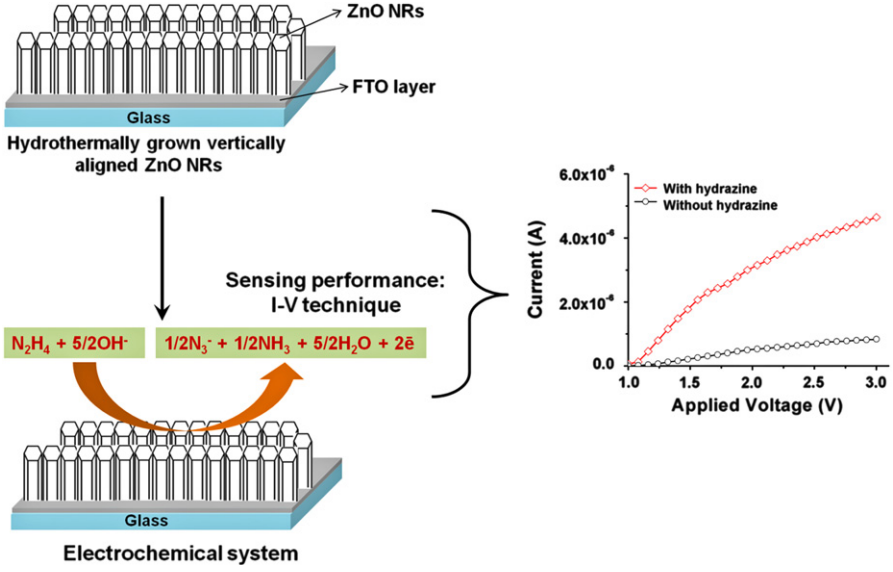

Fig. 6. Schematic illustration of the fabricated hydrazine chemical sensor and the *I–V* characteristics of vertically aligned ZnO NRs modified hydrazine chemical sensor in the absence and presence of hydrazine in 10 ml of 0.3 μM 0.1 M PBS solution.

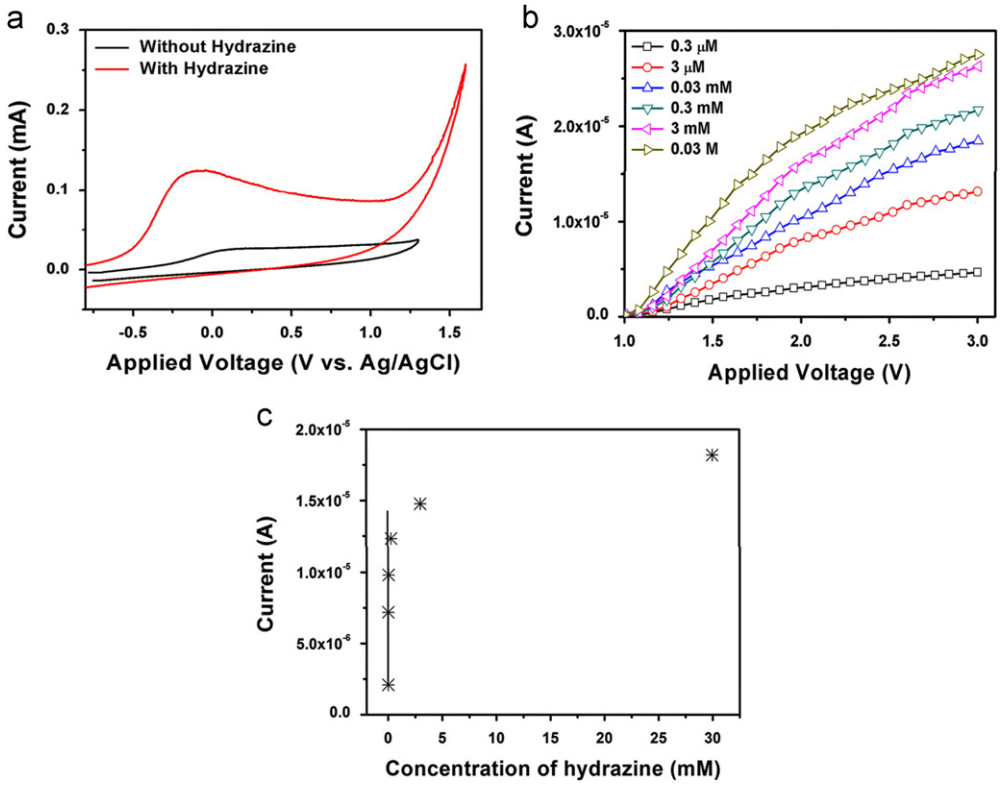

Fig. 7. (a) Typical cyclovoltammetry curve of vertically aligned ZnO NRs without and with hydrazine, (b) the *I–V* characteristics of vertically aligned ZnO NRs modified hydrazine chemical sensor in hydrazine concentration range of 0.3 μM to 0.03 M in 10 ml of 0.1 M PBS solution and (c) calibration curve of current versus concentrations of the fabricated hydrazine sensor.

significantly high sensitivity of $\sim 4.42446 \times 10^{-5}$ A mM^{-1} cm^{-2} and a detection limit of $\sim$515.7 μM with a correlation coefficient (R) of $\sim$0.73297 and a short response time of 10 s. From the CV measurements, the vertically aligned ZnO NRs electrode exhibits increased current with high height of anodic peak in presence of hydrazine, confirming the involvement of high electron transfer process via high electrocatalytic activity of the electrode.

Acknowledgments

This work is fully supported by NRF Project # 2011-0029527. This work was also supported by the Research Funds of Chonbuk National University in 2009. We would like to thank Mr. Kang Jong-Gyun, Center for University-Wide Research Facilities, Chonbuk National University for his cooperation in obtaining TEM images.

References

[1] K. Yamada, K. Yasuda, N. Fujiwara, Z. Siroma, H. Tanaka, Y. Miyazaki, T. Kobayashi, Electrochem. Commun. 5 (2003) 892–896.
[2] S. Amlathe, V.K. Gupta, Analyst 113 (1988) 1481–1483.
[3] C. Zhang, G. Wang, Y. Ji, M. Liu, Y. Feng, Z. Zhang, B. Fang, Sens. Actuators B 150 (2010) 247–253.
[4] Y.Y. Liu, I. Schmeltz, D. Hoffman, Anal. Chem. 46 (1974) 885–889.
[5] A. Savafi, M.A. Karimi, Talanta 58 (2002) 785–792.
[6] H.J. Zhang, J.S. Huang, H.Q. Hou, T.Y. You, Electroanalysis 21 (2009) 1869–1874.
[7] L. Zheng, J.F. Song, Talanta 79 (2009) 319–326.
[8] (a) S. Ameen, M.S. Akhtar, Y.S. Kim, O.B. Yang, H.S. Shin, Electrochim. Acta 56 (2011) 1111–1116;
(b) Z. Jing, J. Wang, F. Li, L. Tan, Y. Fu, Q. Li, J. Nanoeng. Nanomanuf 2 (2012) 133–142.
[9] S. Ameen, M.S. Akhtar, H.K. Seo, Y.S. Kim, H.S. Shin, Chem. Eng. J. 187 (2012) 351–356.
[10] S. Ameen, M.S. Akhtar, Y.S. Kim, O.B. Yang, H.S. Shin, Colloid Polym. Sci. 289 (2011) 415–421.
[11] S. Ameen, M.S. Akhtar, Y.S. Kim, O.B. Yang, H.S. Shin, Microchim. Acta 172 (2011) 471–478.
[12] A. Umar, S.H. Kim, Y.B. Hahn, Curr. Appl. Phys. 8 (2008) 793–797.
[13] A. Umar, M.M. Rahman, M. Vaseem, Y.B. Hahn, Electrochem. Commun. 11 (2009) 118–121.
[14] (a) A. Umar, M.S. Chauhan, S. Chauhan, R. Kumar, G. Kumar, S.A. Al-Sayari, S.W. Hwang, A. Al-Hajry, J. Colloid Interface Sci. 363 (2011) 521–528;
(b) P.K. Samanta, Sci. Adv. Mater. 4 (2012) 219–226.
[15] S. Baskoutas, G. Bester, J. Phys. Chem. C 115 (2011) 15862–15867.
[16] A. Chrissanthopoulos, S. Baskoutas, N. Bouropoulos, V. Dracopoulos, P. Poulopoulos, S.N. Yannopoulos, Photonics Nanostruct. 9 (2011) 132–139.
[17] Y.F. Gao, M. Nagai, T.C. Chang, J.J. Shyue, Cryst. Growth Des. 7 (2007) 2467–2471.
[18] E. Galoppini, J. Rochford, H.H. Chen, G. Saraf, Y.C. Lu, A. Hagfeldt, G. Boschloo, J. Phys. Chem. B 110 (2006) 16159–16161.
[19] A. Hu, F. Wu, J. Liu, J. Jiang, R. Ding, X. Li, C. Cheng, Z. Zhu, X. Huang, J. Alloys Compd. 507 (2010) 261–266.
[20] G.N. Dar, A. Umar, S.A. Zaidi, S. Baskoutas, S.H. Kim, M. Abaker, A. Al-Hajry, S.A. Al-Sayari, Sci. Adv. Mater. 3 (2011) 901–906.
[21] A.A. Ibrahim, G.N. Dar, S.A. Zaidi, A. Umar, M. Abaker, H. Bouzid, S. Baskoutas, Talanta 93 (2012) 257–263.
[22] G.N. Dar, A. Umar, S.A. Zaidi, S. Baskoutas, S.W. Hwang, M. Abaker, A. Al-Hajry, S.A. Al-Sayari, Talanta 89 (2012) 155–161.
[23] Y. Ni, J. Zhu, L. Zhang, J. Hong, CrystEngComm 12 (2010) 2213–2218.
[24] B. Fang, C.H. Zhang, W. Zhang, G.F. Wang, Electrochim. Acta 55 (2009) 178–182.
[25] A. Umar, M.M. Rahman, Y.B. Hahn, J. Nanosci. Nanotechnol. 9 (2009) 4686–4691.
[26] A. Al-Hajry, A. Umar, Y.B. Hahn, D.H. Kim, Superlatt. Microstruct. 45 (2009) 529–534.
[27] S. Ameen, M.S. Akhtar, S.G. Ansari, O.B. Yang, H.S. Shin, Superlatt. Microstruct. 46 (2009) 872–880.
[28] R.A. Laudise, E.D. Kolb, A.J. Caporason, J. Am. Ceram. Soc. 47 (1964) 9–12.
[29] (a) J.H. Sun, S.Y. Dong, J.L. Feng, X.J. Yin, X.C. Zhao, J. Mol. Catal. A: Chem. 335 (2011) 145–150;
(b) P. Poulopoulos, S. Baskoutas, S.D. Pappas, C.S. Garoufalis, S.A. Droulias, A. Zamani, V. Kapaklis, J. Phys. Chem. C 115 (2011) 14839–14843;
(c) S. Baskoutas, P. Poulopoulos, V. Karoutsos, M. Angelakeris, N.K. Flevaris, Chem. Phys. Lett. 417 (2006) 461–464.
[30] (a) A. Dhakshinamoorthy, P. Visuvamithiran, V. Tharmaraj, K. Pitchumani, Catal. Commun. 16 (2011) 15–19;
(b) M. Abaker, A. Umar, S. Baskoutas, G.N. Dar, S.A. Zaidi, S.A. Al-Sayari, A. Al-Hajry, S.H. Kim, S.W. Hwang, J. Phys. D: Appl. Phys. 44 (2011) 425401–425405.
[31] S. Ameen, M.S. Akhtar, H.S. Shin, Chem. Eng. J. 195 (2012) 307–313.

[32] R.M. Silverstein, F.X. Webster, Spectrometric Identification of Organic Compounds, John Wiley & Sons, New York, NY, USA, 1998.
[33] C. Roy, S. Byrne, E. McGlynn, J.P. Mosnier, E. de Posada, D.O. Mahony, J.G. Lunney, M.O. Henry, B. Ryan, A.A. Cafolla, Thin Solid Films 436 (2003) 273–276.
[34] J. Serrano, F.J. Manjon, A.H. Romero, F. Widulle, R. Lauck, M. Cardona, Phys. Rev. Lett. 90 (2003) 055510–055514.
[35] C.D. Wagner, W.M. Riggs, L.E. Davis, J.F. Moulder, G.E. Muilenberg, Handbook of X-ray Photoelectron Spectroscopy, Perkin Elmer, Eden Prairie, 1979.
[36] W.J. Li, E.W. Shi, W.Z. Zhong, Z.W. Yin, J. Cryst. Growth 203 (1999) 186–196.
[37] J.C.C. Fan, J.B. Goodenough, J. Appl. Phys. 48 (1977) 3524–3531.
[38] A. Umar, M.M. Rahman, S.H. Kim, Y.B. Hahn, Chem. Commun. (2008) 166–168.
[39] S.K. Mehta, K. Singh, A. Umar, G.R. Chaudhary, S. Singh, Sci. Adv. Mater. 3 (2011) 962–967.
[40] J. Liu, Y. Li, J. Jiang, X. Huang, Dalton Trans. 39 (2010) 8693–8697.
[41] A. Umar, M.M. Rahman, Y.B. Hahn, Talanta 77 (2009) 1376–1380.